ce/papers Proceedings in civil engineering

Ernst & Sohn A Wiley Brand

ORIGINAL ARTICLE

eurosteel AMSTERDAM 2023

Ernst & Sohn A Wiley Brand

Digital-Image-Correlation for Simulating Cyclic Local Buckling in Steel Beams

Selimcan Ozden[1] | Albano de Castro e Sousa[1] | Dimitrios Lignos[1]

Correspondence

Mr. Selimcan Ozden
École Polytechnique Fédérale de Lausanne (EPFL)
RESSLAB
Rte Cantonale
1015 Lausanne
Email: selimcan.ozden@epfl.ch

[1] EPFL, Ecublens, Switzerland

Abstract

Nonlinear continuum finite element (CFE) analyses rely on accurate multiaxial constitutive law formulations along with reliable imperfection patterns for simulating nonlinear geometric instabilities in steel members under mechanical loading. Validations of these models usually rely on conventional measurements of macroscopic parameters (e.g., displacement and strain field). It is common to use global deformation characteristics (e.g., deduced moment versus chord rotation) for model validation purposes of steel members exhibiting inelastic cyclic local buckling. The reason is that measurements from conventional strain gauge readings are not deemed to be reliable well before the onset of local buckling. This is potentially problematic when the accurate prediction of local strain demands is essential. This paper discusses the experimental results from a steel beam instrumented with a digital image correlation (DIC) system and how optical measurements acquired from DIC can be used to benchmark a CFE model representation of this beam. It is shown that while different CFE model types simulate accurately the moment rotation relationship of the steel beam, local strain demand predictions could vary considerably between model types. The results suggest that DIC measurements can inform the selection of proper imperfection patterns to be used in CFE models for the reliable estimation of inelastic strain demands.

Keywords

Digital image correlation, Nonlinear continuum finite element analyses, Inelastic cyclic straining, Initial geometric imperfections, Local geometric instabilities, Steel moment resisting frames, Dissipative zones, Local engineering demand parameters

1 Introduction

Capacity-designed steel moment resisting frames (MRFs) absorb the energy due to seismic loading through flexural yielding at the beam ends and at the base of first story columns. Depending on the amplitude of the inelastic deformations within the dissipative zone(s) along with local slenderness requirements of the respective steel cross-sections, inelastic local buckling is likely to occur even at modest lateral drift demands [1]. Therefore, seismic performance assessment methodologies of structures rely on the availability of numerical models that simulate inelastic local buckling. For this purpose, different model fidelities have been proposed throughout the years ranging from phenomenological (e.g., [2]) fiber-based (e.g., [3]) and continuum finite element [4-5] approaches.

Local engineering demand parameters (EDPs), such as inelastic strain demands can be estimated through validated continuum finite element (CFE) models. Acquired data from physical experiments exhibiting instabilities including their synergistic action (e.g., interaction of lateral torsional buckling with local buckling) should be used for this purpose.

Prior related work has mostly focused on the ability of CFE models to capture the global behavior of steel members (e.g., deduced moment-chord rotation, axial shortening) [4- 5]; however, the accurate prediction of local strain and deformation demands has been overlooked. This is important for predicting ductile fracture due to ultra-low cycle fatigue [6]. Strain measurements are typically acquired with strain gauge sensors. In this case, the reliability of strain measurements becomes questionable at strain ranges above the yield strain. Other potential problems relate to the bonding of the strain gauge(s) with the corresponding measurement surface through adhesives. These typically fail at strain amplitudes, which are much smaller than strain demands at the onset of nonlinear geometric instabilities, such as local buckling.

https://doi.org/10.1002/cepa.2671

Digital image correlation (DIC) [7] is an advanced optical measurement technique that may be used to validate the ability of CFE models to accurately prognosticate the behavior of steel members in the post-buckling regime.

In prior work [8] the importance of the mesh type and size, the residual stress pattern, the initial geometric imperfections, and constitutive model formulation have been stressed. A common simulation practice for simulating inelastic cyclic local buckling has been the use of shell elements [4-5, 8-9]. However, the accuracy of inelastic strain demand predictions within the local buckling region is challenging to assess. In addition to the finite element type (e.g., shell versus solid), the corresponding imperfection shape and amplitude for tracing the onset of local buckling could influence the strain demands in the post-buckling range.

This paper presents the findings from an experimental program on cantilever steel beam that was instrumented with conventional sensors as well as a DIC system to inform the validity of CFE models in the large deformation range. The paper presents a summary of recommendations on how to accurately trace both global and local EDPs within steel members exhibiting inelastic cyclic local buckling. In the subsequent sections, the test specimen is presented along with the employed instrumentation, the CFE model validation and a discussion of the primary results.

2 Test specimen and employed loading protocol

The test specimen features a IPE330 steel beam with a reduced beam section (RBS). A schematic representation of the steel beam is shown in Figure 1 along with its basic geometric properties. The steel beam was made of S355J2+AR steel (i.e., nominal yield strength of 355MPa, minimum of 27 joules impact energy at -20°C, AR stands for the rolled delivery condition). The center of the RBS was situated 188 mm from the top surface of a 60 mm thick column base. The fabrication process involved complete joint penetration (CJP) welds between the beam flanges and the steel base plate that respected the execution class 3(EXC3) according to EN1090-2 [10].

The employed lateral loading protocol featured a symmetric cyclic loading history up to 4% story drift ratio [11], which was then followed by a collapse-consistent loading protocol [12].

2.1 Test setup and instrumentation

The test setup, which is shown in Figure 2a, featured a rigid spreader beam that was mounted on the strong floor. The test specimen was mounted on the spreader beam through pre-loaded 10.9 structural steel bolts. The test specimen was braced laterally at 960 mm away from the column base. Finally, the imposed loading protocol was applied in displacement control through a 1000kN servo hydraulic actuator that transferred the horizontal load to the strong floor through a steel plate shear wall.

The test specimen was instrumented with two pairs of string potentiometers to measure the lateral displacement and beam axial shortening, respectively, six vertical linear variable differential transformers (LVDTs) to measure the vertical displacement of the spreader beam and the base plate. These were used to calculate their in-plane rotations, which were subtracted from the total applied displacement. Four horizontal LVDTs were also installed to measure the potential slip of the spreader beam and the base plate. Two inclinometers were also installed to measure in-plane and out-of-plane rotations of the test specimen. Uniaxial strain gauges were installed at one side of the steel beam (see Figure 2b) to measure the longitudinal strain demands throughout loading at two levels. The first one was located at the RBS center (i.e., 188 mm above the top of the base plate); the second one at 50 mm away from the base plate, (i.e., outside the heat affected zone of the CJP welds).

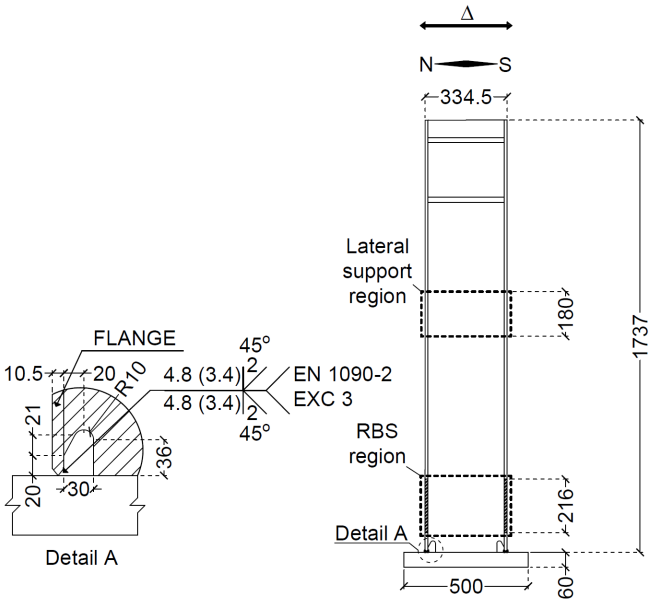

Figure 1 Test specimen geometry and weld details

The DIC system was employed to measure the 3-dimensional displacement field of the web over a height of 396 mm from the base. A random spectacle black-dotted pattern was featured for this purpose to aid the DIC measurements. Figure 2c shows the image acquisition points within the critical region (white-painted area) of the test specimen.

2.2 Deduced data of interest

The primary measurements of interest entail the deduced moment-chord rotation relation (i.e., global EDP) of the steel beam after the removal of the friction in the steel clevises as discussed in [9]. With regards to the DIC measurements, they were post-processed by means of a displacement analysis using the Vic-3D software [13]. After determining the area of interest, a subset size of 33x33 pixels was defined to enable tracking of grey scales with a confidence of 0.01 pixel for a predetermined expected noise level. According to [14], the step size was selected as one quarter of the subset size (8 pixel). The filter size was decided after conducting a virtual strain gauge sensitivity analysis in Vic-3D to minimize the bias error [7]. The logarithmic (Hencky) strains and the out-of-plane deformation within the RBS region were then extracted. Selected experimental results are reported in the subsequent sections along with meaningful comparisons from numerically simulated data.

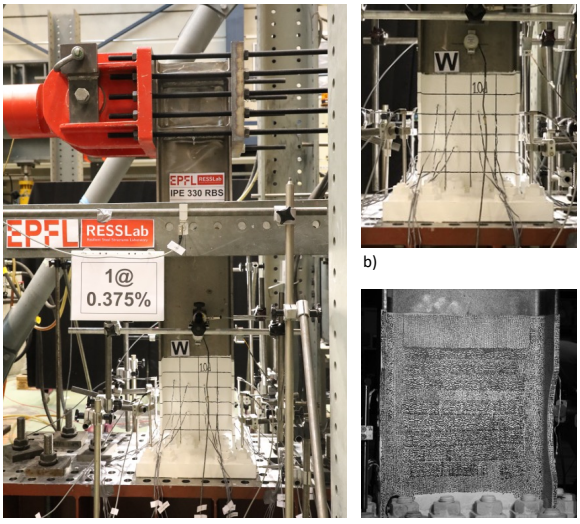

Figure 2 Experimental setup and basic instrumentation

3 Continuum finite element model

3.1 Modeling approach

The test specimen was modeled using the commercial finite element software ABAQUS (version 6.19-1) [15]. Multiaxial plasticity was considered with the Updated Voce-Chaboche (UVC) material model [16]. The parameters of this model are based on uniaxial cyclic coupon tests that were manufactured from the web and the flanges of the IPE330. Figure 3 shows a sample comparison between the simulated and measured data for one of the cyclic coupon tests under a strain-based loading history as per [17].

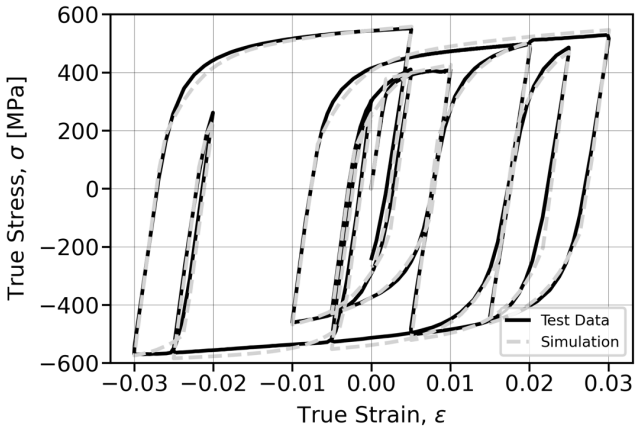

Figure 3 Comparison between test data and simulation for uniaxial strain-based loading protocol

Figure 4 depicts the boundary conditions of the CFE model. The lateral loading was applied through in-plane displacement ($\delta_{y,1}$). The rotational ($\theta_{y,1}$, $\theta_{z,1}$) and out-of-plane displacement ($\delta_{x,1}$) degrees of freedom were restrained to simulate the boundary conditions. The out-of-plane displacement ($\delta_{x,2}$) in Region 2 (see Figure 4) was restrained due to the presence of the lateral bracing. Residual stresses due to flame cutting within the RBS region were not considered.

Local geometric imperfections were considered by scaling and superimposing the local elastic buckling modes of the RBS IPE330 according to [4]. The amplitude of the nonlinear geometric imperfections was considered based on prior work in [8].

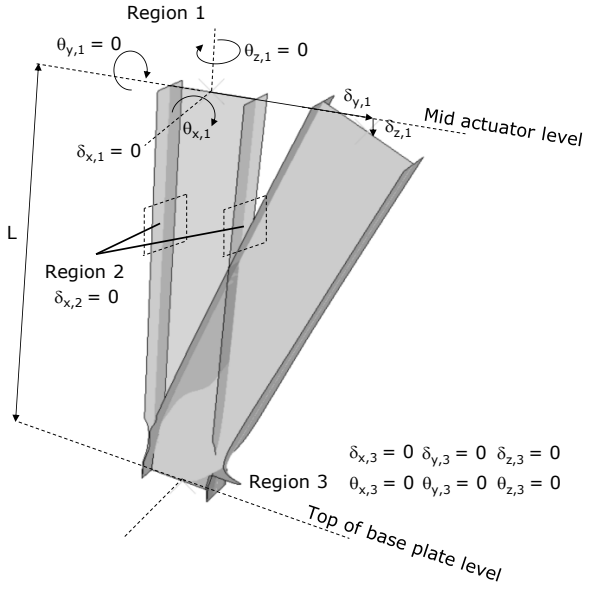

Figure 4 Boundary conditions of the CFE model

Two initial geometric imperfection patterns were considered in the CFE simulations. These patterns are shown in Figure 5. Patterns 1(= Mode 1 + Mode 2) and 2 (= Mode 1 - Mode 2) are consistent with the manufacturing limits of current standards [18]. The geometric imperfections were assigned based on buckling mode superposition as discussed in [4].

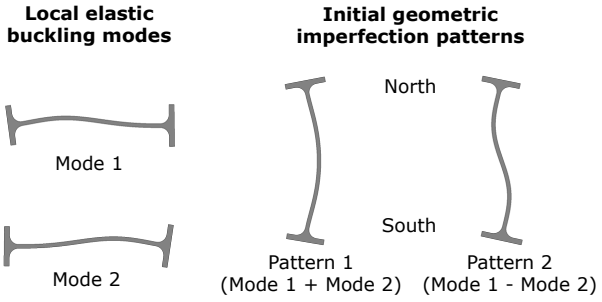

Figure 5 Pattern 1 and Pattern 2 initial geometric imperfections

Four model types were considered. The first and second types considered linear shell elements with reduced integration (S4R). The third and fourth types featured quadratic solid elements with reduced integration (C3D20R). The shell models employed an element size of 12.5 mm according to [8]. The mesh size of the solid elements featured 6 mm within the RBS region and three elements through the flange and web thickness.

4 Results and Discussion

Figure 6 depicts the deduced moment-chord rotation comparisons between the four model type simulations and the test results. Particularly, Model A and B featured shell elements with initial geometric imperfections of Patterns 1 and 2, respectively. Similarly, Models C and D featured solid elements with initial geometric imperfections of Patterns 1 and 2, respectively (see Figure 5).

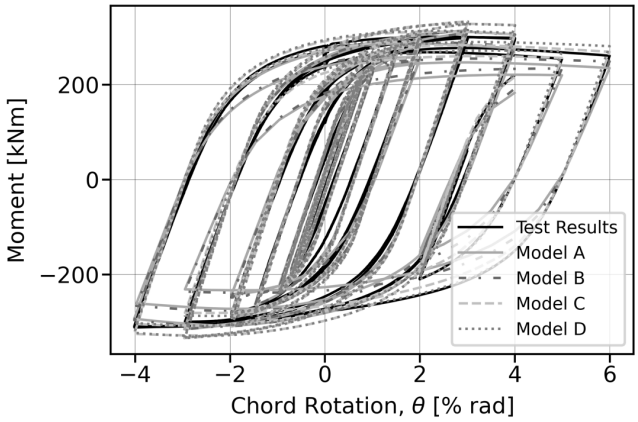

Figure 6 Global response comparison between the test results, shell, and solid simulations

Prior to the onset of local buckling, the overall hysteretic response of the test specimen is depicted well regardless of the model type. Conversely, Models C and D depict the onset and progression of local buckling more accurately than Models A and B. This is attributed to the explicit consideration of the k-area and fillet radius in the model representation with solid elements.

From the same figure, the deduced moment-chord rotation relation is not sensitive to the considered geometric imperfection shape. Figure 7 shows the relative error between the measured moment and those simulated from Models A, to D versus the cumulative chord rotation, θ_{cum}. The relative error in the post-buckling regime is indeed on the order of 35% when shell elements are considered.

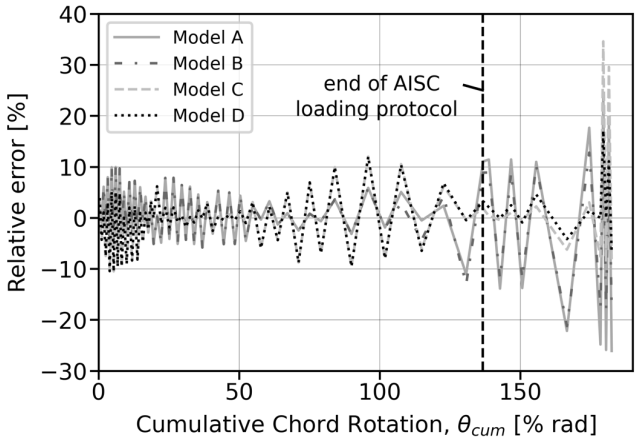

Figure 7 Relative error between measurement and simulations from Models A, B, and C

Figure 8 shows the analysis locations of interest at the center of the RBS region. The DIC and strain gauge measurements were taken from the east and west side of the web, respectively.

Figures 9 and 10 demonstrate a comparison of the strain histories from the two measurement systems and those obtained from the four models only at Loc-1 (see Figure 8) due to brevity. From these figures, up until the first excursion of 4% rad (commences after 100% cumulative chord rotation), the measured and simulated strain values are similar. Figure 10 shows that the strain gauge acquisition interrupts because the signal goes out of the pre-defined measurement range. From the same figure, the strain gauge signal is completely lost at 117 % cumulative chord rotation.

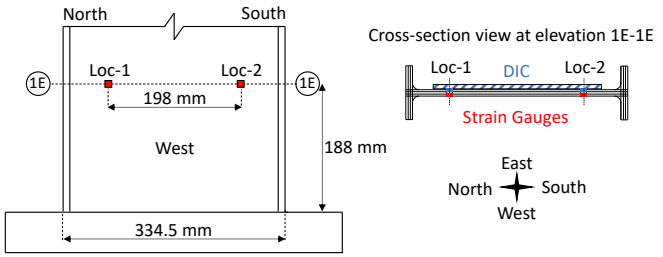

Figure 8 Location of measurement and analyses points on the member through elevation and at the cross-section

Figure 9 suggests that Models A and C do not depict accurately the inelastic strain evolution in the post-buckling regime, whereas Models B and D are in closer agreement with the DIC measurements. Model A and C are in close agreement. This indicates the importance of depicting more accurately the initial geometric imperfection pattern.

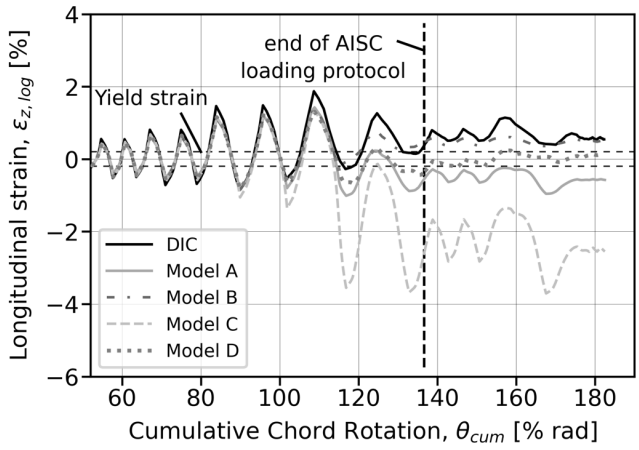

Figure 9 Logarithmic longitudinal strain history up until the first phase of the collapse-consistent protocol; Loc 1: DIC measurements and simulations (East side)

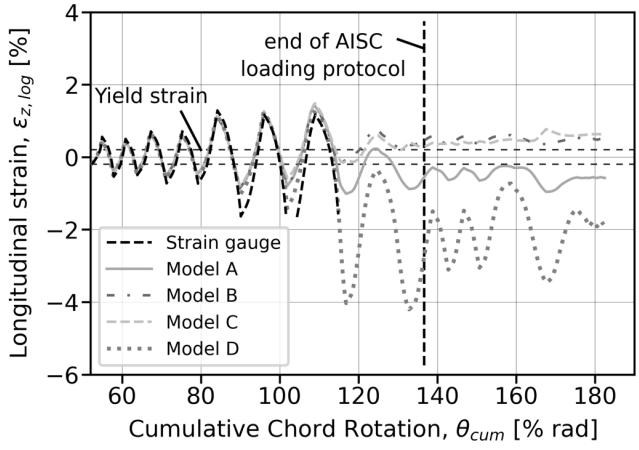

Figure 10 Logarithmic longitudinal strain history up until the first phase of the collapse-consistent protocol; Loc 1: strain gauge measurements and simulations (West side)

Similarly, Figure 10 suggests that Model D predicts well

the strain gauge measurements up until the strain gauge signal went out of range. Conversely, Models A, B and C depart from the strain gauge measurements at 117% cumulative chord rotation.

To further substantiate the findings, Figure 11 and Figure 12 show a comparison between the measured and simulation results for the out-of-plane deformation versus cumulative chord rotation at Loc-1 and Loc-2, respectively. The out-of-plane deformations from the DIC measurements are simulated accurately with Model D at Loc-1. However, the simulation results from Models A, B and C depart from those of the DIC measurements after the first excursion of the 4% loading amplitude (i.e., onset of local buckling). Although all model predictions agree with the out-of-plane deformations from the DIC measurements as depicted in Figure 12, the DIC measurements are simulated best with Model D.

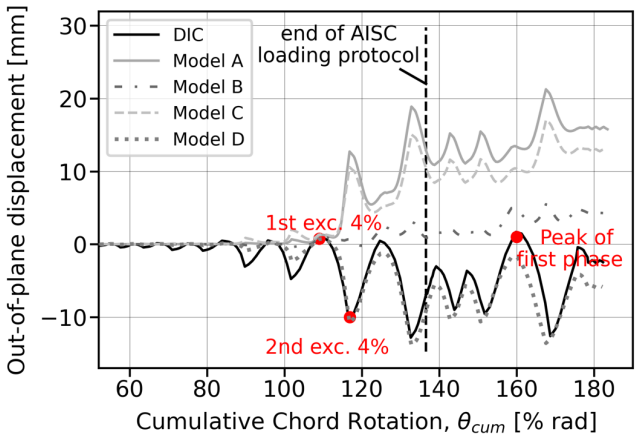

Figure 11 Out-of-plane displacement history up until the first phase of the collapse-consistent protocol; Loc 1: DIC measurements and simulations (East side)

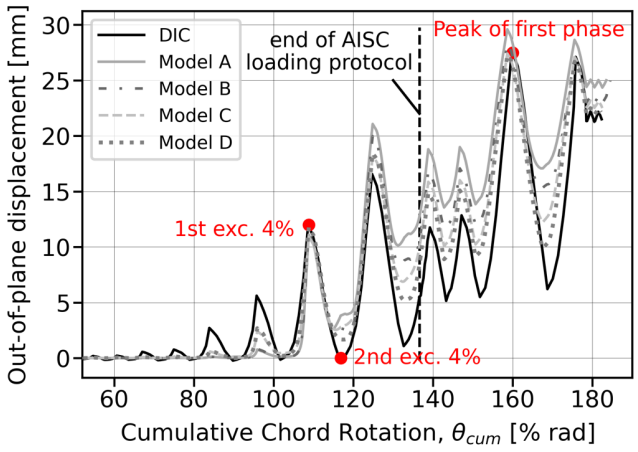

Figure 12 Out-of-plane displacement history up until the first phase of the collapse-consistent protocol; Loc 2: DIC measurements and simulations (East side)

Figure 13 depicts the out-of-plane displacement profile of the web based on the DIC measurements and Models A, B, C and D at the 1E-1E cross-section at different loading excursions of the employed loading history. The loading direction is noted in the same figures. Referring to Figure 13a, the simulated deformation patterns match relatively well with the measurements right at the onset of local buckling (i.e., first excursion of 4% rad). Upon further loading (i.e., second excursion of 4% rad), Models A and C predict the opposite deformation pattern from that of the measurements. This is attributed to the assumed imperfection pattern (1 or 2). In this case, Pattern 2 is deemed to be the right one to be considered. Finally, at the peak excursion of the collapse consistent protocol (see Figure 13c) demonstrates that Model D still predicts relatively well the out-of-plane deformation pattern of the web, whereas Model C overpredicts the web deformations. However, the figure suggests that the depending on the direction of loading (North-South or South-North) the web deformation may be opposite to that of the measurements (see Figure 13b) or in the same direction (see Figure 13c). This is also demonstrated in Figure 11 throughout the entire loading history.

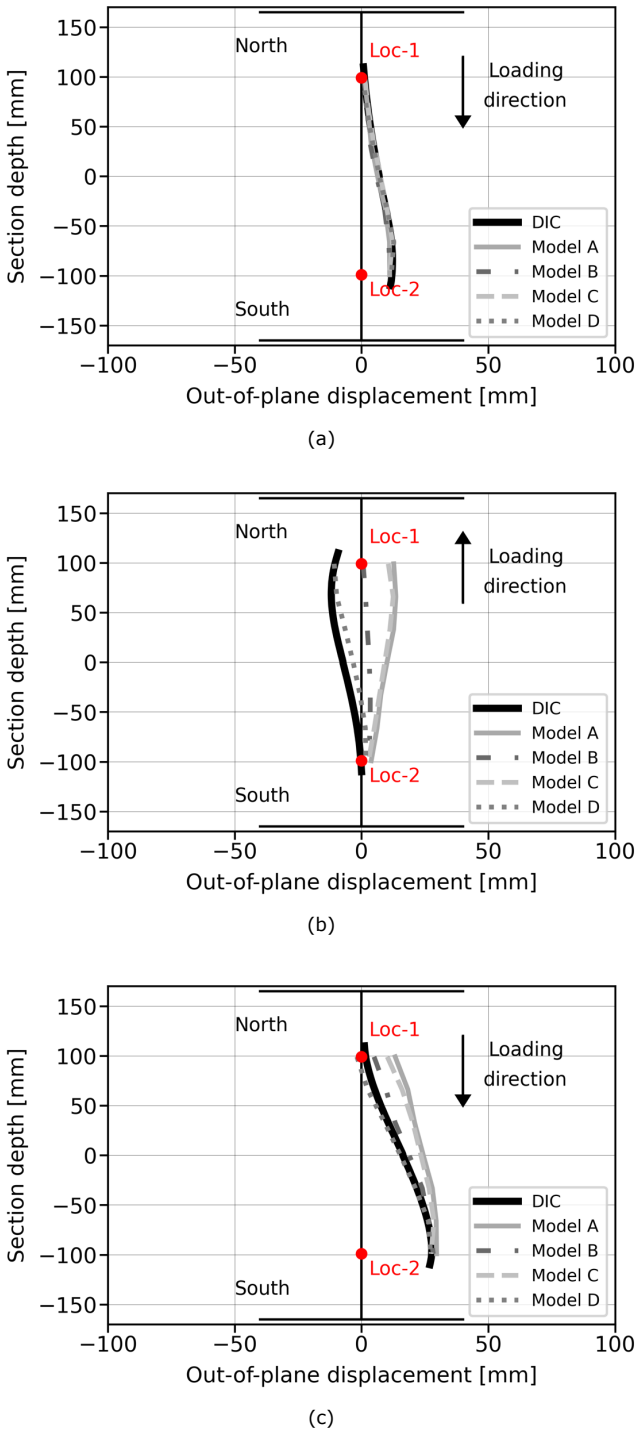

Figure 13 Comparisons between DIC measurements and simulation

predictions for out-of-plane displacement at cross-section 1E-1E (mid-RBS); (a) first excursion of 4% rad; (b) second excursion of 4% rad; (c) peak excursion of collapse-consistent protocol

5 Conclusions

This paper investigates the effective utilization of data acquired from a Digital Image Correlation (DIC) system for the accurate simulation of inelastic cyclic local buckling within dissipative zones of steel beams. The primary focus is on the modeling assumptions within a continuum finite element (CFE) model so as the strain and out-of-plane displacement fields may be accurately predicted far into the post-buckling regime. For this purpose, a cantilever beam was tested under quasi-static cyclic loading. The steel beam featured a reduced beam section (RBS), which was thoroughly instrumented. The primary findings are summarized as follows:

- The type of imperfection does not strongly influence the global response (i.e., deduced moment-chord rotation). However, the type of imperfection has a strong influence on the predicted local response (i.e., out-of-plane displacement and strain demands).
- The simulation results suggest that for the examined test specimen, A CFE model with solid elements and a Pattern 2 initial geometric imperfection appears to match well both the deformation shape and amplitude along with the strain demands prior and after the onset of local buckling within the RBS region.
- Three elements through thickness in a solid element model type should be used for the examined case to trace accurately the strain demands throughout the entire loading history.
- The global response of the cantilever beam is not sensitive to the CFE model type (i.e., shell versus solid). However, the explicit consideration of the k-area of the wide flange structural shape appears to be important in the post-buckling regime. Thus, solid elements would be more appropriate for simulating the post-buckling behavior of the examined steel member.

References

[1] Uang, C.-M.; Bruneau, M. (2018) *State-of-the-Art Review on Seismic Design of Steel Structures*. Journal of Structural Engineering 144, H. 4, p. 03118002, https://doi.org/10.1061/(ASCE)ST.1943-541X.0001973.

[2] Ibarra, L.F.; Medina, R.A.; Krawinkler, H. (2005) *Hysteretic Models that Incorporate Strength and Stiffness Deterioration*. Earthquake Engineering & Structural Dynamics 34, H. 12, pp. 1489–1511, https://doi.org/10.1002/eqe.495.

[3] Suzuki, Y.; Lignos, D.G. (2020) *Fiber-based Hysteretic Model for Simulating Strength and Stiffness Deterioration of Steel Hollow Structural Section Columns Under Cyclic Loading*. Earthquake Engineering & Structural Dynamics 49, H. 15, pp. 1702–1720, https://doi.org/10.1002/eqe.3324.

[4] Elkady, A.; Lignos, D.G. (2015) *Analytical Investigation of the Cyclic Behavior and Plastic Hinge Formation in Deep Wide-flange Steel Beam-columns*. Bulletin of Earthquake Engineering 13, H. 4, pp. 1097–1118, https://doi.org/10.1007/s10518-014-9640-y.

[5] Sediek, O.A.; Wu, T.-Y.; Chang, T.-H.; McCormick, J.; El-Tawil, S. (2021) *Measurement, Characterization, and Modeling of Initial Geometric Imperfections in Wide-Flange Steel Members Subjected to Combined Axial and Cyclic Lateral Loading*. Journal of Structural Engineering 147, H. 9, p. 04021120, https://doi.org/10.1061/(ASCE)ST.1943-541X.0003086.

[6] Smith, C.; Ziccarelli, A.; Terashima, M.; Kanvinde, A.; Deierlein, G. (2021) *A Stress-weighted Ductile Fracture Model for Steel Subjected to Ultra Low Cycle Fatigue*. Engineering Structures 245, p. 112964, https://doi.org/10.1016/j.engstruct.2021.112964.

[7] iDICs (2018) *A Good Practices Guide for Digital Image Correlation*. International Digital Image Correlation Society. https://doi.org/10.32720/idics/gpg.ed1/print.format

[8] Hartloper, A. (2021) *Reduced-order Models for Simulating Coupled Geometric Instabilities in Steel Beam-columns Under Inelastic Cyclic Straining*. Ph.D. Thesis, EPFL.

[9] Cravero, J. (2016) *Experimental Evaluation of Steel Wide-flange Columns in Moment-resisting Frames Under High Axial Load and Lateral Drift Demands*. Ph.D. Thesis, McGill University.

[10] CEN (2018) *Execution of Steel Structures and Aluminium Structures Technical Requirements for Steel Structures. EN 1090-2*. Brussels: European Commitee for Standardization.

[11] AISC (2010) *Seismic Provisions for Structural Steel Buildings. ANSI/AISC 341-10*. Chicago: American Institute of Steel Construction.

[12] Suzuki, Y.; Lignos, D.G. (2020) *Development of Collapse-consistent Loading Protocols for Experimental Testing of Steel Columns*. Earthquake Engineering & Structural Dynamics 49, H. 2, pp. 114–131, https://doi.org/10.1002/eqe.3225.

[13] Vic-3D (2010) *Vic-3D*. Irmo, SC, USA: Correlated Solutions.

[14] Correlated Solutions (2022) *Subset, Step Size and Filter Selection*, *Technical Articles*.https://correlated.kayako.com/article/44-subset-step-size-and-strain-filter-selection

[15] ABAQUS (2019) *ABAQUS - FEA/CAE*. RI, USA: Dassault Systems Simulia Corp.

[16] Hartloper, A.R.; de Castro e Sousa, A.; Lignos, D.G. (2021) *Constitutive Modeling of Structural Steels: Nonlinear Isotropic/Kinematic Hardening Material Model and Its Calibration*. Journal of Structural Engineering 147, H. 4, p. 04021031, https://doi.org/10.1061/(ASCE)ST.1943-541X.0002964.

[17] de Castro e Sousa, A.; Suzuki, Y.; Lignos, D. (2020) *Consistency in Solving the Inverse Problem of the Voce-Chaboche Constitutive Model for Plastic Straining*. Journal of Engineering Mechanics 146, H. 9, p. 04020097, https://doi.org/10.1061/(ASCE)EM.1943-7889.0001839.

[18] CEN (1993) *Structural Steel I and H Sections: Tolerances on Shape and Dimensions. EN 10034*. Brussels: European Commitee for Standardization.